Internal Magnetic Turbulence Measurement in Plasma by Cross Polarization Scattering

X. L. Zou, L. Colas, M. Paume, J. M. Chareau, L. Laurent, P. Devynck, and D. Gresillon*

Association EURATOM-Commissariat à l'Energie Atomique sur la Fusion Contrôlee, Département de Recherches sur la Fusion Controlée SPPF CE Cadarache BPN°1, 13108 St Paul lez Durance, France

(Received 3 October 1994)

For the first time, the internal magnetic turbulence is measured by a new cross polarization scattering diagnostic in the Tore Supra tokamak. The principle of this experiment is presented. It is based on the polarization change or mode conversion of the electromagnetic wave scattered by magnetic fluctuations. A strong correlation between the internal magnetic fluctuation and the additional heating is observed, contrary to the edge fluctuations. The observed fluctuations increase linearly with the poloidal beta number β_p in the L-mode confinement regime.

PACS numbers: 52.70.Gw, 52.25.Sw, 52.35.Ra

The electron thermal diffusivity measured in tokamaks is much larger than that predicted by neoclassical theory. In the standard models for this anomalous transport, the loss mechanism for particles and energy in the plasma is attributed to microturbulence [1]. Experimentally, the electrostatic turbulence or density fluctuations $\tilde{n}$ have been intensively studied in tokamaks (edge and core), and the results were not always consistent to show that the electrostatic turbulence determines the internal energy confinement [2]. The magnetic turbulence $\tilde{B}$ is at present measured only at the edge by magnetic coils [3], or indirectly by the analysis of the runaway electron transport [4]. The internal measurement of $\tilde{B}$ is then indispensable for the clarification of its role in the anomalous heat transport. In this Letter, we present a new diagnostic—the cross polarization scattering diagnostic, which is the first attempt to measure the internal $\tilde{B}$.

The cross polarization scattering has been intensively investigated by different authors [5–8]. A simple qualitative description is given here. From an eletromagnetic wave $\mathbf{E}_i$ of frequency ω_i, the scattered field $\mathbf{E}_s$ resulting from $\tilde{n}, \tilde{B}$ is given by

$$-\nabla \times (\nabla \times \mathbf{E}_s) + \left(\frac{\omega_i}{c}\right)^2 \left(1 - \frac{\sigma}{i\varepsilon_0 \omega_i}\right) \mathbf{E}_s = -i\mu_0 \frac{\partial \mathbf{J}^{(2)}}{\partial \mathbf{t}}, \quad (1)$$

where σ is the unperturbed conductivity tensor. Using a simple nonlinear fluid model, the induced current $\mathbf{J}^{(2)}$ for the cold plasma limit is given by

$$\mathbf{J}^{(2)} = \frac{i\varepsilon_0 \omega_{pe}^2}{\omega_i} \frac{\tilde{n}}{n_e} \mathbf{E}_i + \frac{\omega_i}{\varepsilon_0 \omega_{pe}^2} \sigma[(\sigma \mathbf{E}_i) \times (\tilde{B}/B)], \quad (2)$$

where ω_{pe} is the plasma frequency and B the static magnetic field. The first term on the right-hand side of Eq. (2), describing the interaction between $\tilde{n}$ and $\mathbf{E}_i$, and being parallel to $\mathbf{E}_i$, gives a scattered wave of the same polarization. This is the usual scattering process for $\tilde{n}$. The second term, describing the interaction between $\tilde{\mathbf{B}}$ and $\mathbf{E}_i$, has a polarization perpendicular to $\mathbf{E}_i$ due to the vectorial product between $\mathbf{E}_i$ and $\tilde{\mathbf{B}}$, and can generate a scattered wave of cross polarization. This phenomenon, called the cross polarization scattering (CPS), is used to measure the magnetic fluctuation in our experiment.

Two eigenmodes exist in tokamaks for wave propagation perpendicular to $\mathbf{B}$: the ordinary mode (O) with polarization parallel to $\mathbf{B}$, and the extraordinary mode ($\mathbf{X}$) with polarization perpendicular to $\mathbf{B}$. The scattering processes described above can be schematically described as follows: $O_i + \tilde{n} \rightarrow O_s$, $O_i + \tilde{B} \rightarrow X_s$ for an incident O wave, and symmetrically $X_i + \tilde{n} \rightarrow X_s$, $X_i + \tilde{B} \rightarrow O_s$ for an incident X wave. In tokamaks, due to the expected value of $\tilde{B}/B$ being lower than $\tilde{n}/n$, the scattered signal from $\tilde{B}$ is estimated to be 10^3 times less than that coming from $\tilde{n}$. To reject the signal scattered by $\tilde{n}$ from the total scattered signal we introduce the polarizing mirror effect (PME). The basic idea is to use the cutoff of the incident wave as a perfect polarizer. This principle is shown in Fig. 1 with the scenario $X_i + \tilde{B} \rightarrow O_s$. An X mode is launched vertically with its cutoff layer in the plasma. The receiver antenna is positioned at the bottom of the torus, while the emitter antenna is at the top. The X

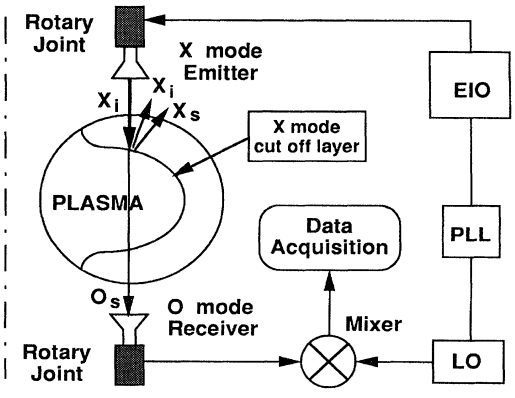

FIG. 1. Diagram of the cross polarization scattering diagnostic. Schematic describing the polarizing mirror effect with the scenario $X_i + \tilde{B} \rightarrow O_s$.

 0031-9007/95/75(6)/1090(4)$06.00

mode cutoff layer reflects the incident X wave and the X wave scattered by $\tilde{n}$, but lets through the O mode converted to $\tilde{B}$. The scattering volume is located between the top plasma edge and the cutoff layer. The fluctuation wave number selected by the Bragg selection rule $k_{\text{fluct}} = k_O - k_X$ is radial rather than poloidal.

The CPS diagnostic consists mainly of a millimeter-wave source and a heterodyne detection system (see Fig. 1). A high mode purity is required for the emitter and receiver antennas in order to optimize the polarization selection. This includes a quasioptic Gaussian system and an accurate positioning system with a motorized rotary joint. The rotary joint allows a match of the antenna electric field direction to that of the total magnetic field at the plasma edge with a precision of 0.36° (1000 steps/rotation). The millimeter-wave source is an extended interaction oscillator (EIO) of 60 GHz ($\lambda_0 =$ 5 mm) with a maximum output power of 70 W. The total losses due to waveguides and millimetric components in the transmission lines are estimated to be -23 dB. The half angle of divergence of the wave beam launched by the antennas into the vacuum is less than 1° and its linear polarization in power is better than -30 dB (10^{-3}). The local oscillator (LO) is a Gunn diode with an output power of 70 mW. The frequency difference between EIO and LO is stabilized at 48 MHz by a phase lock loop. The signal from the plasma is then mixed with that from the LO by a balanced mixer. The absolute sensitivity of this detection system is $\text{NEP}_H = 10^{-18}$ W/Hz.

In tokamaks two intrinsic plasma effects can affect the wave polarization: (1) the eigenmode mixing effects such as the Faraday and Cotton-Mouton effects which can be avoided by the separation of the two modes thanks to the polarizing mirror and (2) the coupling between the two modes due to the magnetic shear [9]. This mode coupling can be important in the adiabatic transition layer at the plasma edge, or near the upper hybrid resonance region [10]. For our cases the coupling rate is estimated to be less than 10^{-4} in both cases and can therefore be neglected. Thus one can consider that each eigenmode propagates independently in the plasma following the local magnetic field. The mode conversion by $\tilde{B}$ occurs locally even though the magnetic field direction changes. Finally, the residual polarization rate is dominated by the alignment of the incident electric field to the magnetic field at the plasma edge, which causes a spurious polarization rate lying between -25 and -30 dB.

The first experiments, presented in Figs. 2 and 3, have been performed with the CPS scenario $X_i + \tilde{B} \rightarrow O_s$. The plasma parameters are helium gas, with a major plasma radius of $R = 2.46$ m and a minor plasma radius of $a = 0.68$ m. The central plasma density and the magnetic field are chosen to have an X mode cutoff in the plasma: $B_0 = 1.82$ T and $n_{e0} = 3.6 \times 10^{19}$ m^{-3}. This cutoff layer is located close to $r/a = 0.85$. The receiver antenna is set with a polarization parallel to the O mode. Figure 2 shows the time evolution of the plasma parameters and the video signal S_v that represents the power directly transmitted through the plasma and detected by the receiver antenna, and then measured by a video detector with a frequency window of 20 kHz. The process used to find the emitting antenna positions includes three phases: (1) for $4 < t < 5$ s, just after the plasma shift from the inner wall to the outboard limiter, the emitting antenna rotates by 360°. During this phase S_v is used to find the antenna position where the O (S_v maximum) or X (S_v minimum) modes are launched. (2) For $5 < t < 6.4$ s the emitter is tuned to the O mode, i.e., the standard forward scattering configuration $O \rightarrow O$. (3) After 6.4 s the emitter is tuned to the X mode, i.e., the CPS configuration $X \rightarrow O$. The difference between the maximum and minimum values of S_v is about 30 dB; i.e., the antenna can be aligned to within 2° of the edge magnetic field by this process. This indicates that the depolarization effect by reflection on the wall is less than -30 dB. Thus the O modes converted by wall depolarization from the X wave scattered by $\tilde{n}$ are

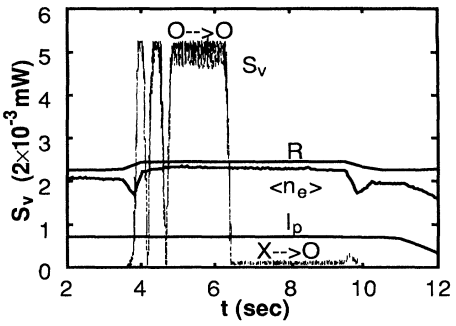

FIG. 2. Time evolution of the plasma current I_p (MA), the major radius R (m), the mean density $\langle n_e \rangle$ (10^{19} m^{-3}), and the direct transmission power S_v (mW).

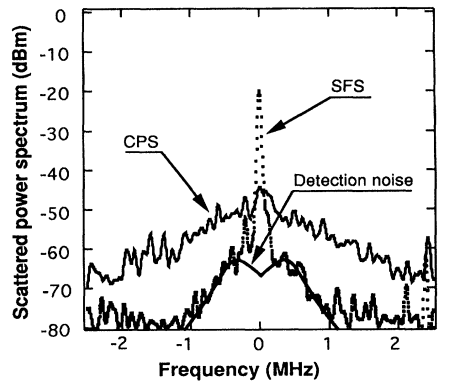

FIG. 3. Turbulence spectra obtained with the CPS configuration (solid), $X_i + \tilde{B} \rightarrow O_s$, and the SFS configuration (dashed), $O_i + \tilde{n} \rightarrow O_s$. $I_p = 0.79$ MA, $B_0 = 1.82$ T, and $n_{e0} = 3.6 \times 10^{19}$ m^{-3}. 0 dB m = 1 mW.

negligible. Polarization analysis by the rotation of the receiver antenna confirms that the received signal is in the O mode, thus excluding the possibility that the received signal is a component of the spurious X mode signal coming directly from the emitter via a multireflection on the wall.

Figure 3 shows the frequency power spectra of the fluctuation, obtained separately from the two scenarios: standard forward scattering (SFS) $O_i + \tilde{n} \rightarrow O_s$ (dashed line), and cross polarization scattering $X_i + \tilde{B} \rightarrow O_s$ (solid line). The large central peak in the SFS case represents the unscattered component of the transmitting wave for $\omega \approx 0$, and the forward scattering by *density fluctuations* with $0 < \omega < 200$ kHz. Note that the central peak has totally disappeared in the CPS case, but a broad spectrum of 2 MHz is observed. This is of course due to the presence of the X mode cutoff in the plasma. The dramatic change in the spectra can be considered to be the signature of the CPS process and can be explained as follows: (a) In the SFS configuration, i.e., the $O \rightarrow O$ forward scattering k_{fluct} $(= k_s - k_i \approx 0)$ is limited to 0.5 cm^{-1}. The drift frequency, defined as $\omega^* = k_{\text{fluct}} T_e / eB_0 L_n \approx 40$ kHz, is in agreement with the observed SFS spectrum. $L_n = n_e/|dn_e/dr|$ is the density scale length. (b) In the CPS configuration two $X \rightarrow O$ scattering processes are observed by the receiver antenna: forward scattering before reflection where k_{fluct} $(= k_O - k_X)$ varies from 0 in the vacuum to ω_i/c $(= 12.56$ cm$^{-1})$ at the cutoff, and backscattering after reflection where k_{fluct} $(= k_O + k_X)$ varies from ω_i/c at the cutoff to $2\omega_i/c$ in the vacuum. Thus the contribution of $\tilde{B}$ from the cutoff layer, estimated to be the dominant effect as was indicated in Ref. [7], is localized at $k_{\text{fluct}} = \omega_i/c$, for which the corresponding $\omega^* \approx 1$ MHz is in agreement with the observed CPS spectrum. On the other hand, the contribution of edge $\tilde{B}$ in the CPS signal is in the low k range, i.e., the low frequency range, or in the large k range $(= 25.12$ cm$^{-1})$ where the fluctuation level is too small. This emphasizes the fact that the CPS signal originates from the cutoff region. Note that the spectrum around 500 kHz in the SFS case, shown by the thick solid line in Fig. 3, is due to the phase noise in the heterodyne detection system, as its level is directly proportional to the received power. Similar features are found for the symmetric case: a low amplitude, broad spectrum for $O_i + \tilde{B} \rightarrow X_s$, and a large central peak with a small base for $X_i + \tilde{n} \rightarrow X_s$. The magnetohydrodynamics (MHD) activity, characterized by a very low wave number and frequency, is not directly measured by our diagnostic. The reason for this is that the dominating k_{fluct} in the CPS signal is very far from that of the MHD.

A simplified scattering equation, allowing us to calculate $\tilde{B}/B$ from the scattered power in Fig. 3, can be expressed in the following form [7]:

$$dP_s = K_s C_R P_{i\,\text{eff}} \Delta\Omega \Delta f \bar{n}_e L r_0^2 u/(1-u)^2 S_b\,, \qquad (3)$$

where K_s is the spatial localization factor, C_R is the loss factor due to refraction, L is the scattering volume length, $\bar{n}_e$ is the mean density in the scattering volume, $P_{i\,\text{eff}}$ is the effective incident power, $\Delta\Omega$ is the solid angle of detection, Δf is the frequency resolution, r_0 is the classical electron radius, and the frequency ratio $u = (\omega_{ce}/\omega_i)^2$. The form factor relative to $\tilde{B}$ is defined as for the density fluctuation S_n [11]:

$$S_b(k,\omega) = \lim_{T,V\rightarrow\infty} \frac{n_e}{TV}\left[\frac{\tilde{\mathbf{B}}(k,\omega)\cdot\tilde{\mathbf{B}}^*(k,\omega)}{B^2}\right]. \qquad (4)$$

S_b has the dimension of a time as S_n. With $dP_s \approx 10^{-5}$ mW, $P_{i\,\text{eff}} = 50$ mW, $\Delta\Omega = 5 \times 10^{-2}$ sr, $\Delta f = 30$ kHz, $r_0 = 2.82 \times 10^{-15}$ m, $\bar{n}_e = 0.7 \times 10^{19}$ m^{-3}, $L = 0.1$ m, $K_s = 3.2$, $C_R = 0.1$, and $u = 0.72$ ($B_0 = 1.82$ T), we find that $S_b \approx 6.2$ s. S_b can then be directly linked to the $\tilde{B}$ correlation function by the Wiener-Kinchine theorem [11]. By integrating this equation over phase space, we obtain

$$\int S_b(k,\omega)\,(d\omega/2\pi)\,dk^3/(2\pi)^3 = n_e[(\tilde{B}/B)^2]. \qquad (5)$$

Assuming that the phase volume corresponding to this fluctuation is given by $\Delta f = 0.5$ MHz, $\Delta k_r \approx \Delta k_\theta \approx 10$ cm^{-1}, and $\Delta k_\parallel \approx 0.07$ cm^{-1}, we find that $\tilde{B}/B \approx 1.2 \times 10^{-4}$. The uncertainty for this estimate is 100%.

A second series of experiments has been performed with the CPS scenario $O_i + \tilde{B} \rightarrow X_s$. The results presented in Fig. 4 are obtained with the same plasma parameters: $R = 2.32$ m, $a = 0.76$ m, $I_p = 1.3$ MA, $B_0 = 3.76$ T, and $n_{e0} = 6.5 \times 10^{19}$ m^{-3}. In this case the CPS signal is localized close to the O mode cutoff layer, i.e., at $r/a = 0.57$. Figure 4(a) shows the time evolution of the different signals in the presence of additional heating [ion cyclotron resonance heating (ICRH)]: the

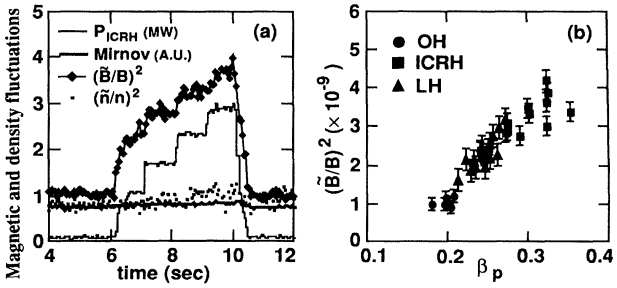

FIG. 4. (a) Time evolution of the different fluctuation signals in the presence of additional heating ICRH (thin solid line): the internal magnetic fluctuations (diamond) are measured by the CPS at 300 kHz in a window of 10 kHz, and the density fluctuations (dot) are measured by CO_2 laser coherent scattering at $k_\theta = 12$ cm^{-1}. Both of these signals are normalized to the Ohmic regime. The edge magnetic fluctuations are measured by the Mirnov coil (thick solid line). $I_p = 1.3$ MA, $B_0 = 3.76$ T, $n_{e0} = 6.5 \times 10^{19}$ m^{-3}. (b) Dependence of the internal magnetic fluctuation as a function of β_p in the L regimes (ICRH, liquid helium).

internal $\tilde{B}$ measured by the CPS diagnostic at 300 kHz in a window of 10 kHz, the edge $\tilde{n}$ measured by CO_2 laser coherent scattering at $k_\theta = 12\ \mathrm{cm}^{-1}$ [12], and the edge $\tilde{B}$ measured by Mirnov coils in a frequency window of 10 kHz. Some observations can be drawn from this figure: A strong correlation between the internal microscopic magnetic turbulence and additional heating is evidenced, while the edge $\tilde{n}$ and edge $\tilde{B}$ (Mirnov coil signal) are insensitive to this heating, as has been observed in several tokamaks. This means that the CPS signal in the high frequency range ($\omega \approx 300$ kHz) is not polluted by the edge fluctuations.

Figure 4(b) displays the internal $\tilde{B}$ as a function of the poloidal beta number β_p. It clearly shows that in the L-mode confinement regime the internal magnetic turbulence increases linearly with β_p: $(\tilde{B}/B)^2 = \kappa(\beta_p - \beta_{p0})$, where $\beta_{p0} \approx 0.15$ and $\kappa \approx 2 \times 10^{-8}$. Thus $\tilde{B}/B \approx (3.2-6.4) \times 10^{-5}$ for this case. This value of $\tilde{B}/B$ measured at $r/a = 0.57$ is compatible with the anomalous electron heat diffusivity measured in Tore Supra ($\chi_e \approx 0.8\ \mathrm{m}^2\mathrm{s}^{-1}$) if we use the quasilinear expression for χ_e due to $\tilde{B}$ [13]. However, τ_E can be directly linked to β_p. In fact by eliminating the injected power P_{tot} in the relations $\tau_E = W/P_{\mathrm{tot}}$ (definition) and $\tau_E \propto I_p P_{\mathrm{tot}}^{-1/2}$ (Goldston [14]), we obtain $\tau_E^{-1} \propto W/I_p^2 \propto \beta_p$. This suggests that in the L regimes the anomalous transport in the core can be caused by the internal magnetic turbulence, which is decoupled from the edge turbulence. We emphasize that the plasma parameters, and hence the location of the cutoff, are constant for the discharges shown in Fig. 4.

In summary, the cross polarization scattering caused by magnetic fluctuations is identified by comparing the fluctuation spectra from the two opposing configurations CPS and SFS. A large spectral broadening effect is observed, which is considered to be the signature of the magnetic turbulence measured using this method. A strong correlation between the internal magnetic fluctuations and additional heating is also observed. In the L regimes, these fluctuations are dissociated from the edge fluctuations (density and magnetic).

The authors gratefully acknowledge the effort of the Tore Supra team for the machine operation and technical support, especially M. Accensi, P. Ouvrier-Buffet, and D. Elbeze.

*Permanent address: Laboratoire PMI (UPR 287 du CNRS), Ecole Polytechnique, 91128 Palaiseua, France.

[1] P. C. Liewer, Nucl. Fusion **25**, 543 (1985).
[2] A. J. Wootton *et al.*, Phys. Fluids B **12**, 2879 (1990).
[3] S. J. Zweben, C. R. Menyuk, and R. J. Taylor, Phys. Rev. Lett. **42**, 1270 (1979).
[4] C. W. Barnes and J. D. Strachan, Phys. Fluids **26**, 2668 (1983).
[5] T. Lehner, D. Gresillon, X. L. Zou, and B. De Gentile, in *Proceedings of the 12th European Conference on Controlled Fusion and Plasma Physics, Budapest* (Petit-Lancy, Switzerland, 1985), Vol. II, p. 644.
[6] T. Lehner, J. M. Rax, and X. L. Zou, Europhys Lett. **8**, 759 (1989).
[7] X. L. Zou, L. Laurent, and J. M. Rax, Plasma Phys. Controlled Fusion **33**(8), 903 (1991).
[8] L. Vahala, G. Vahala, and N. Bretz, Phys. Fluids B **4**, 619 (1992).
[9] V. L. Ginzburg, *Propagation of Electromagnetic Wave in Plasmas* (Gordon and Breach, New York, 1961).
[10] I. Fidone and G. Granata, Nucl. Fusion **11**, 133 (1971).
[11] G. Bekefi, *Radiation Processes in Plasma* (John Wiley, New York, 1966).
[12] P. Devynck, X. Garbet, and C. Laviron, *et al.*, Plasma Phys. Controlled Fusion **35**, 65 (1993).
[13] A. B. Rechester and M. N. Rosenbluth, Phys. Rev. Lett. **40**, 38 (1978).
[14] R. J. Goldston, Plasma Phys. Controlled Fusion **26**, 87 (1984).